Interpretation®

Coherence attribute applications on seismic data in various guise - Part 1

Journal:	*Interpretation*
Manuscript ID	INT-2018-0006
Manuscript Type:	Technical Paper (if no special section applies)
Date Submitted by the Author:	05-Jan-2018
Complete List of Authors:	Chopra, Satinder; TGS, Reservoir Services; Marfurt, Kurt; University of Oklahoma, College of Earth and Energy;
Keywords:	attributes, interpretation, reservoir characterization, faults
Subject Areas:	Reservoir characterization/surveillance

Coherence attribute applications on seismic data in various guise - Part 1

Satinder Chopra[†] *and Kurt J. Marfurt*[+]

[†] *Arcis Seismic Solutions, TGS, Calgary*; [+] *The University of Oklahoma, Norman*

Abstract

The iconic coherence attribute is very useful for geologic feature imaging such as faults, deltas, submarine canyons, karst collapse, mass transport complexes, and more. Besides its preconditioning, the interpretation of discrete stratigraphic features on seismic data is also limited by its bandwidth, where in general the data with higher bandwidth yields crisper features than data with lower bandwidth. Some form of spectral balancing applied to the seismic amplitude data can help in achieving such an objective, so that coherence run on spectrally balanced seismic data yields a better definition of the geologic features of interest. The quality of the generated coherence attribute is also dependent in part on the algorithm employed for its computation. In the eigenstructure decomposition procedure for coherence computation, spectral balancing equalizes each contribution to the covariance matrix, and thus yields crisper features on coherence displays. There are other ways to *modify the spectrum of the input data* in addition to simple spectral balancing, including the amplitude-volume technique, taking the derivative of the input amplitude, spectral bluing, and thin-bed spectral inversion. We compare some of these techniques, and show their added value in seismic interpretation in this work, which forms Part 1 of the more elaborate exercise that has been carried out. In Part 2 of the paper, we discuss how different spectral components derived from

the input seismic data allow interpretation of different scales of discontinuities, what additional information is provided by coherence computed from narrow band spectra, and finally the different ways to integrate them.

Introduction

Since its introduction at the 1995 SEG Annual Meeting, the coherence attribute has come a long way. As an iconic attribute, it finds its place in most workstation interpretation software packages, and for good reason. Because three-dimensionality is an essential ingredient of the coherence volume computation, the geologic feature imaging is done well without any bias. Thus, faults that run parallel to reflector strike seen on time slices, radiate from a salt dome, or appear en echelon faults, all appear clearly on coherence displays. Similarly, as beaches and deltas are seen clearly on coherence displays, a better idea of progression and retreat is possible while trying to reconstruct the sequence stratigraphy of the area. The same is true about interpreting mudflows, submarine canyons, and understanding depositional stratigraphy, that may be unidentifiable on seismic reflection data even on close scrutiny. Other features that may be added to this list would be karst collapse and mass transport complexes. Umpteen case studies have been published in the last two-and-a-half decades to describe and illustrate the advantage of bringing the coherence attribute into the seismic interpretation workflow.

In general, the quality of an attribute display is dependent on the algorithm employed for its computation, and the quality of the seismic amplitude data from which it is generated. Various algorithms for coherence computation have been developed in the last twenty-five years, starting from the crosscorrelation technique, and the quality of the coherence attribute

generated has improved considerably since then. We discuss the semblance, eigenstructure and energy ratio coherence computation methods, and show that the energy ratio coherence algorithm is better than the semblance algorithm, which is available on most workstation packages.

Even when the seismic data have been migrated reasonably well and are multiple free, they are often contaminated with random noise, coherent mismigrated shallow diffraction noise, migration operator aliasing artifacts, and occasional noise spikes. Often, the interpreter can address such noise through simple structure-oriented mean and median or slightly more sophisticated principal component filtering. Whatever noise suppression workflow is adopted, care must be taken such that faults and other discontinuities in the seismic amplitude data are not smeared.

The interpretation of discrete stratigraphic features on seismic data is limited by its bandwidth. Seismic data that have a higher bandwidth yield crisper and more detailed images than the same data with lower bandwidth. Usually, a cursory generation of frequency spectra for the seismic data being interpreted shows that the amplitudes of higher frequencies show a gradual roll off, unless the data have been spectrally balanced during processing. The latter step could be a concern for amplitude preservation for AVO applications and impedance inversion.

Computation of the first or second derivative of the seismic data skew the frequency spectrum towards the higher frequencies, though at the cost of the low frequency amplitudes, and thus the data exhibit a higher resolution. Chopra and Marfurt (2017) demonstrate such an application. Taking the first derivative of seismic data does two things – it multiplies each

frequency component by the frequency f resulting in spectral 'bluing', and it rotates the phase of the data by 90^o, so that the peaks and troughs of the amplitudes are transformed into zero crossings. Similarly, taking the second derivative of the seismic data would further shift the frequency spectrum to the higher frequency side and rotate the phase by 180^o.

In the application of all of these processes, we are essentially modifying the frequency spectrum of the input seismic data, but within the bandwidth of the input seismic data. There are however, workflows available that can extend the bandwidth of the seismic data, and such data exhibit enhanced resolution. Of course, one has to be careful about the amplitude preservation aspect of the process in each case for specific objectives, which may not be critical for geometrical attribute computation. Some form of spectral balancing or bandwidth extension of the seismic data prior to attribute computation, helps in achieving such an objective.

Vernengo and Trinchero (2015) described the application of amplitude-volume-technique (AVT) workflow that aids seismic interpretation. It entails the calculation of the root-mean-square (RMS) of the seismic amplitudes in a definite analysis and then rotate the phase of the data by –90^o, by using the mathematical operation of Hilbert Transform. Such a calculation of the input seismic data yields somewhat higher amplitudes of the frequencies in the bandwidth of the data.

We demonstrate the application of coherence attribute on input seismic data, on the first and second derivatives run on the same data, and then after application of spectral balancing and

bandwidth extension. Finally, we also include the application of coherence attribute on seismic data that has been passed through the AVT workflow.

Alternative coherence algorithms

The different coherence algorithms that have been proposed over time are the cross-correlation-based (Bahorich and Farmer, 1992), semblance-based (Marfurt et al., 1998), variance-based coherence (Pepper and Bergano, 2005), eigenstructure-based (Gersztenkorn and Marfurt, 1999), prediction error filter-based (Bednar, 1998) and gradient structure tensor-based (Bakker, 2003). These algorithms vary in how they handle seismic character variability and thus have different sensitivities to geology, spectral bandwidth and seismic noise. Out of these the most commonly available algorithms available in workstation software packages are the semblance and some form of eigenstructure decomposition. Here we restrict our analysis to semblance and the energy-ratio coherence, the latter of which is based on a variation of the eigenstructure approach.

Semblance

Marfurt et al. (1998) described the M-trace semblance coherence estimate as

$$C_{semb} = \frac{\sum_{k=-K}^{K}\left\{\frac{1}{M}\sum_{m=1}^{M}[d(t_k,x_m,y_m)]\right\}^2 + \left\{\frac{1}{M}\sum_{m=1}^{M}[d^H(t_k,x_m,y_m)]\right\}^2}{\sum_{k=-K}^{K}\frac{1}{M}\left\{\sum_{m=1}^{M}[d(t_k,x_m,y_m)]^2\right\} + \frac{1}{M}\left\{\sum_{m=1}^{M}[d^H(t_k,x_m,y_m)]^2\right\}}, \quad (1)$$

where **d** is the seismic amplitude, $\mathbf{d}^{\mathrm{H}}$ is its Hilbert transform, and the indices represent the different samples in the computation window in the inline (x), crossline (y) and the time (t) directions. The input data consist of *M* traces of length 2*K*+1 samples centered about the analysis point aligned with structural dip. Equation 1 can be interpreted as the ratio of the energy of the average trace (in the numerator) to the average of the energies of each of the traces (in the denominator).

Eigenstructure Coherence

The eigenstructure method is based on the eigenvectors and eigenvalues of the covariance matrix as was introduced by Gersztenkorn and Marfurt (1999), though several details have been modified since then. The covariance matrix, **C**, is constructed from the analytic trace composed of the original data, **d**, and its Hilbert transform, $\mathbf{d}^{\mathrm{H}}$, along structural dip, to prevent 'structural leakage', corresponding to zero crossings (Chopra and Marfurt, 2007):

$$C_{mn} = \sum_{k=-K}^{K} [d(t_k, x_m, y_m)d(t_k, x_n, y_n) + d^H(t_k, x_m, y_m)d^H(t_k, x_n, y_n)]. \quad (2)$$

As most of the covariance matrices we come across in attribute analysis are square, they are decomposed into non-negative eigenvalues, and so can be written in the forms as shown below.

$$\mathbf{C}\mathbf{v}^j = \lambda_j \mathbf{v}^{kj}, \quad (3)$$

where **C** is an *M* by *M* square covariance matrix, λ_j is the j^{th} eigenvalue, and $\mathbf{v}^j$ is the corresponding eigenvector.

The eigenstructure coherence described by Gersztenkorn and Marfurt (1999) was simply given as the ratio of the first (and by definition, the largest) eigenvalue to the sum of all the eigenvalues of the matrix:

$$C_{eigen} = \frac{\lambda_{max}}{\sum_{j=1}^{J} \lambda_j}. \quad (4)$$

Marfurt (2006) described the principal component structure-oriented filtering, where the principal component filter first constructs a covariance matrix from the 2K+1 sample vectors, and then computes eigenvectors prior to cross-correlating it with the center sample vector. Such a procedure provides a means of computing a principal component filtered version of the data, in terms of $\mathbf{d}_{PC}$ and $\mathbf{d}_{PC}^{H}$.

The energy ratio coherence is thus a slightly more general computation given as:

$$C_{Energy\ ratio} = \frac{\sum_{k=-K}^{+K} \sum_{m=1}^{M} \{[d_{PC}(t_k, x_m, y_m)]^2 + [d_{PC}^{H}(t_k, x_m, y_m)]^2\}}{\sum_{k=-K}^{+K} \sum_{m=1}^{M} \{[d(t_k, x_m, y_m)]^2 + [d^{H}(t_k, x_m, y_m)]^2\}}. \quad (5)$$

In the above mathematical expression, the numerator can be interpreted as the energy of the weighted principal component filtered analytic traces, and the denominator as the sum of the energy of the analytic traces or total energy. In simple notation, the energy ratio coherence may be given as:

$$C_{Energy\ ratio} = \frac{E_{coh}}{E_{tot}}. \quad (6)$$

The comparative performance of semblance and eigenstructure algorithms on real data was demonstrated by Gersztenkorn and Marfurt (1999). In Figure 1 we depict the comparison between the semblance and energy-ratio coherence. Notice the sharp, crisp and more continuous definition of the lineaments seen on the energy-ratio display.

Consequently, all the examples of coherence shown in Part 1 and 2 of this paper are generated using the energy-ratio algorithm.

Subsampling of seismic data

Seismic data are usually processed at the sample rate at which they are acquired, and typically it is 2 ms. For large data volumes, such as those acquired in the offshore areas, seismic data are generally processed at 4 ms sample interval so as to cut down on the time and processing cost. The general rule of thumb is that going coarser results in loss of information in the data. A sample interval of 2 ms may be acceptable for routine type of interpretation work. However, in the interest of high-resolution or precision work, subsampling, may be required. Reducing the sample interval to half its value can prevent any loss of information, or rather help in restoring some finer detail that is not generally seen at the input sample interval. Of course, this would generate double the number of samples per trace, and hence double the size of the 3D seismic data volume.

Subsampling is usually resorted to for data undergoing spectral balancing or bandwidth extension. We generated a version of the input data volume at half the sample rate (1ms) and then put it through spectral balancing, followed by energy ratio coherence computation.

Although one may be able to reduce the vertical size of the coherence analysis window in ms to take advantage of the increased vertical resolution, we kept the data analysis windows for our seismic data volumes the same size in order to make a more direct comparison of the effect of alternative spectral modification techniques

Spectral balancing of input seismic data

By spectral balancing we refer to a processing workflow or a technique that modifies or flattens the frequency spectrum of the data. Simply computing the first derivative of the seismic amplitudes skews the frequency spectrum towards higher frequencies, still within the bandwidth of the data. Similarly, application of the second derivative on the seismic data skews the frequency spectrum to the higher frequency side some more, though at the cost of the amplitudes of lower frequencies. In Figure 2a, we show a segment of an inline from a 3D seismic volume from central Oklahoma, US. The frequency spectrum for the exhibited time window is shown to the right. The equivalent sections from the first derivative, second derivative are shown in Figure 2b and c. Notice, how the frequency spectra are skewed to the higher frequencies side in both cases, and the higher resolution seen on the seismic sections.

Helmore (2009) proposed a frequency split structure oriented filtering workflow, where a single dip-azimuth computation from the broadband is used to apply the structure-oriented filtering to a suite of bandpass filtered versions of the input seismic data. Each output passband can then be boosted to a common output level as is typically done in a whitening process. Thereafter, the results are recombined but as it is a trace by trace computation, the amplitude preservation may be a concern. This workflow flattens the frequency spectrum, but is confined

to the bandwidth of the data that is input to the process. In Figure 3a we show the equivalent section to those shown in Figure 2, after spectral balancing using Helmore's (2009) workflow. The input seismic data was split into five frequency bands within the 10-20-70-80 Hz bandwidth, and put through spectral balancing. As the frequency spectrum is somewhat flattened the section exhibits higher resolution compared with the input seismic section shown in Figure 2a.

Chopra et al., (2011) demonstrated that if the input seismic data are spectrally balanced, or if its frequency bandwidth is extended somehow, the resulting volumes could lead to higher discontinuity detail. Thin-bed spectral inversion (Chopra et al., 2006; Chopra et al., 2008) is a process that removes the time-variant wavelet from the seismic data and extracts the reflectivity to image thicknesses below seismic resolution using a matching-pursuit variant of sparse-spike inversion. In addition to enhanced image of thin-reservoirs, the frequency-enhanced images have proven useful in mapping subtle onlaps and offlaps, thereby facilitating the mapping of parasequences and the direction of sediment transport. Besides viewing the spectrally broadened seismic data in the form of reflectivity, it can be filtered back to any desired bandwidth that filter panel tests indicate, adding useful information for interpretational purposes. In Figure 3b we show an equivalent segment of a seismic section from the data volume obtained by filtering the thin-bed reflectivity to the same bandwidth as the input seismic data. The frequency spectrum for the dataset is also shown to the right of the image. We notice that the data shown in Figure 3b exhibits more frequency content, and detailed definition of faults and fractures. While the seismic data shown in section seen in Figure 3a and b look similar, their equivalent coherence sections exhibit differences. The coherence section

in Figure 3b shows crisp vertical lineaments and an overall higher resolution. Seismic attributes generated on spectrally balanced input data, or when this frequency bandwidth is extended, exhibit more discontinuity detail (Chopra et al., 2011). Coherence attribute computation performed on spectrally balanced data yield higher detail about faults and fractures. Figure 3c shows the equivalent result from the bandwidth extended (10-20-110-120 Hz) seismic data volume exhibiting higher resolution than the sections shown in Figure 3a and b.

We generate energy ratio coherence on different versions of the input seismic data that we generated and have discussed above. A comparison is made in terms of stratal slices shown earlier, just above the Silurian Hunton Limestone marker, which is a platform carbonate in the area that has undergone significant erosion and karstification within the study area. Equivalent coherence stratal slices to those shown in Figure 1 are shown in Figure 4, with coherence on input data in Figure 4a, input data with structure-oriented filtering (Figure 4b), the first derivative computed on data in Figure 4b (Figure 4c), and second derivative computed on data in Figure 4b shown in Figure 4d. Notice, coherence on first and second derivative of seismic amplitude brings out more discontinuity detail on the displays.

Similarly, equivalent stratal slices to those shown in Figure 4 are shown in Figure 5, but coherence generated on data with spectral balancing using Helmore (2009) workflow in Figure 5a, as well as thin-bed reflectivity inversion in Figure 5b. Coherence stratal slices from data subsampled to half its sample interval is shown in Figure 5c, and finally coherence generated on input data put through bandwidth extension using thin-bed reflectivity inversion in Figure 5d. Notice, spectral balancing brings out more discontinuity detail in the display. The definitions seem better-defined with the Helmore (2009) workflow, and even better with thin-bed

reflectivity inversion workflow. Subsampling the input data adds a little crispier detail to the lineaments and frequency bandwidth extension using thin-bed reflectivity inversion adds even more resolution to the display.

Amplitude volume technique attributes

Vernengo and Trinchero (2015) described the application of amplitude volume technique (AVT) to seismic data for enhancing and focusing the subsurface geologic elements, in terms of faults, unconformities, channel edges and thus helping with their interpretation. The AVT attributes was first proposed by Bulhões (1999) and elaborated upon by way of application by Bulhões and de Amorin (2005). The AVT attribute is obtained by calculating the RMS amplitude from the seismic amplitudes in a sliding window down the trace (i.e. calculating the square root of the average of the sum of the squares of the amplitudes). This step is followed by rotating the phase of the data by -90^o, through the application of Hilbert transform. The RMS computation (squaring, averaging and taking square root) makes all the amplitudes positive, but the nonlinearity introduced therein modifies the frequency spectrum, enhancing it at the higher end. The -90^o phase rotation exercised next changes all the amplitudes into positive and negative values. In Figure 6 we show a segment of a section from the input seismic data and its equivalent AVT section, as well as the equivalent section through the coherence run on the AVT data. By looking at the amplitude spectrum of the AVT data, we can conclude that the amplitudes of the lower frequencies are higher than the amplitudes of the higher frequencies, which are seen as extended. Notice, the pseudo-relief introduced in the process, which makes the interpretability of the AVT data much better. In Figure 7 we show a coherence stratal slice from the AVT volume. We notice at once that the coherence on data with AVT shows all

discontinuities more focused, perhaps due to the more pronounced lower frequency content, which in some cases could offer convenience in interpretation.

Conclusions

We have demonstrated the application of coherence attribute on seismic data and its various guises in the form of derived data volumes comprising the first derivative, the second derivative, frequency balancing as well as thin-bed reflectivity inversion workflows, and frequency bandwidth extension using thin-bed reflectivity inversion workflow. In each of these cases the frequency spectra of the input data are modified. On comparison of the equivalent stratal slice coherence displays, we infer the following:

1. If the original data spectrum is biased towards the low part of the spectrum, computing the first or second derivatives provides a quick-and-dirty means to approximate spectral balancing. In this case, coherence computed on the first and second derivative seismic data volumes exhibit higher lineament detail than just the coherence on input seismic data.
2. Computation of squares (in semblance) and crosscorrelations (in forming a covariance matrix) is a nonlinear process. For this reason, linearly subsampling the input seismic data to half its value may generate finer lineaments on the coherence displays not seen on the original data volume.
3. Extension of frequency bandwidth yields more lineament detail.
4. Coherence run on the versions of the data discussed above after AVT shows pronounced definition of lineaments and thus could be used in their interpretation.

Acknowledgements

We wish to thank Arcis Seismic Solutions, TGS, Calgary for permission to present this work.

References

- Bahorich, M. S., and S. L. Farmer, 1995, 3-D seismic coherency for faults and stratigraphic features: The Leading Edge, **14**, 1053–1058.
- Bakker, P., 2003, Image structure analysis for seismic interpretation: Ph.D. thesis, Technische Universiteit Delft.
- Bednar, J. B., 1998, Least-squares dip and coherency attributes: The Leading Edge, **17**, 775–776.
- Bulhoes, E. M., 1999, Tecnica “Volume de Amplitudes” para mapeamento de feicoes estruturais: Anais do VI Congresso Internacional da Sociedade Brasileira de Geofisica (in Portuguese).
- Bulhoes, E. M., and W. de Amorin, 2005, Principio da sismocamada elementar e sua aplicacao a tecnica de volume de amplitudes (TecVa): Anais Ninth International Congress of the Brazilian Geophysical Society (in Portuguese).
- Chopra, S, J. P. Castagna, O. Portniaguine, 2006, Seismic resolution and thin-bed reflectivity inversion, CSEG RECORDER, **31**, 1, 19-25.
- Chopra, S., and K. J. Marfurt, 2007, Seismic attributes for prospect identification and reservoir characterization, Geophysical Development Series, SEG.

- Chopra, S., J. P. Castagna and Y. Xu, 2008, Thin-bed reflectivity inversion and some applications, First Break, **27**, 27-34.
- Chopra, S., S. Misra and K. J. Marfurt, 2011, Coherence and curvature attributes on preconditioned seismic data, The Leading Edge, **21**, 386-393.
- Chopra, S., and K. J. Marfurt, 2017, Enhancing seismic discontinuity attributes with creative workflows, AAPG Explorer, **38**, 20-21.
- Fahmy, W. A., G. Matteucci, J. Parks, M. Matheney, and J. Zhang, 2008, Extending the limits of technology to explore below the DHI floor; successful application of spectral decomposition to delineate DHIs previously unseen on seismic data: 78 Annual International Meeting of the SEG, Expanded Abstracts, 408-412.
- Gersztenkorn, A. and K. J. Marfurt, 1999, Eigenstructure-basd coherence computations as an aid to 3D structural and stratigrahic mapping: Geophysics, **64**, 1468-1479.
- Helmore, S., 2009, Dealing with noise – improving seismic whitening and seismic inversion workflows using frequency split structurally oriented filters, 77th Annual International Meeting, SEG, Expanded Abstracts, 3367-3371.
- Marfurt, K. J., R. L. Kirlin, S. H. Farmer, and M. S. Bahorich, 1998, 3-D seismic attributes using a running window semblance-based algorithm: Geophysics, **63**, 1150–1165.
- Marfurt, K. J., 2006: Robust estimates of reflector dip and azimuth: Geophysics, **71**, P29-P40.
- Pepper,R., and G. Bejarano, 2005, Advances in seismic fault interpretation automation, AAPG Search and Discovery Article 40170,

http://www.searchanddiscovery.com/documents/2005/pepper/, accessed 1st November, 2017.

- Vernengo, L. and E. Trinchero, 2015. Application of amplitude volume technique attributes, their variations, and impact. The Leading Edge, **25**, 1246-1253.

Captions

Figure 1: Comparison of stratal slice displays just above the Hunton Limestone marker (shown along line AA' in Figure 2) through coherence volumes generated using (a) semblance, and (b) energy-ratio algorithms using analytic traces and the same 5-trace by 20-ms analysis window oriented along structural dip. Green arrows indicate zones of improved fault continuity using energy-ratio coherence. Red arrows indicate zones of greater noise in the semblance coherence. Overall, the energy-ratio coherence slices exhibit crisper, more detailed lineaments than the semblance coherence for this geologic formation. *(Data courtesy: TGS, Houston)*

Figure 2a: Vertical slices along line AA' (top) the original 3D seismic volume and (bottom) the corresponding coherence volume. The spectrum ranges between 10 and 80 Hz but is biased towards the low frequencies. The black dashed-line indicates the top of the Hunton Limestone. *(Data courtesy: TGS, Houston)*

Figure 2b: Vertical slices along line AA' through (top) the first derivative of the seismic amplitude and (bottom) the corresponding coherence volume. The effect of the first derivative is to flatten the spectrum in the 10-80 Hz range of the signal. *(Data courtesy: TGS, Houston)*

Figure 2c: Vertical slices along line AA' through through (top) the second derivative of the seismic amplitude and (bottom) the corresponding coherence volume. The effect of the second derivative is to skew the spectrum towards the higher frequencies in the 10-80 Hz range of the signal. *(Data courtesy: TGS, Houston)*

Figure 3a: Vertical slices along line AA' through through (top) seismic amplitude after spectral balancing 10-20-70-80 Hz using Helmore's (2009) workflow and (bottom) the corresponding coherence volume. Unlike derivative operators, spectral balancing preserves the original phase of each spectral component. *(Data courtesy: TGS, Houston)*

Figure 3b: Vertical slices along line AA' through through (top) seismic amplitude after spectral balancing to 10-20-70-80 Hz using thin-bed reflectivity inversion and (bottom) the corresponding coherence volume. *(Data courtesy: TGS, Houston)*

Figure 3c: Vertical slices along line AA' through through (top) seismic amplitude after bandwidth extension to 10-20-110-120 Hz and (bottom) the corresponding coherence volume. *(Data courtesy: TGS, Houston)*

Figure 4: Stratal slices just above the Hunton marker through coherence volumes generated from (a) the original seismic amplitude data, and the seismic amplitude data after (b) structure-oriented filtering, (c) application of the first derivative (b), and (d) application of the second derivative. (b). Green arrows indicate fault details in coherence computed from the first and second derivative amplitude volumes that we interpret to be associated with the lower frequencies. *(Data courtesy: TGS, Houston)*

Figure 5: Stratal slices just above the Hunton marker through coherence volumes generated from (a) the original seismic amplitude data, with spectral balancing using Helmore's (2009) workflow, (b) spectral balancing using thin-bed reflectivity inversion, (c) spectral balancing using thin-bed reflectivity inversion subsampled to half sample interval, and (d) bandwidth extension using thin-bed reflectivity inversion to 10-20-110-120 Hz. Notice, spectral balancing bring out more discontinuity detail in the display. Subsampling input seismic data as well as bandwidth extension using thin-bed reflectivity extract even greater detail on these images. *(Data courtesy: TGS, Houston)*

Figure 6: Vertical slices along line AA' through (a) the original seismic volume, (b) Amplitude Volume Transform (AVT) volume, and (c) the equivalent line through the coherence volume on AVT volume. The AVT extends both the high and low frequency content of the original data, whereby the lower frequencies provide a pseudo-relief or "outcrop" appearance favored by many interpreters. The amplitudes of lower frequencies are higher than those for the higher frequencies, and thus it does give a low frequency look. *(Data courtesy: TGS, Houston)*

Figure 7: Stratal slices just above the Hunton marker through coherence volumes generated from the AVT volume. This image emphasizes the larger, through-going faults seen by the lower frequencies, and is thus complementary to images obtained using spectral balancing and bandwidth extension. *(Data courtesy: TGS, Houston)*

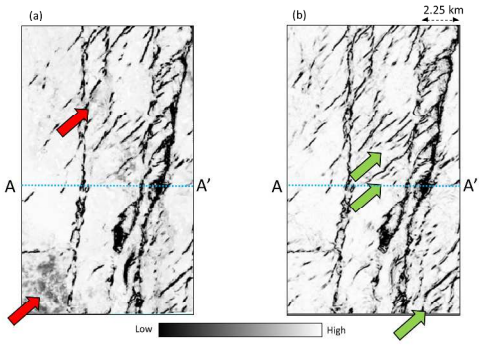

Figure 1

Figure 1: Comparison of stratal slice displays just above the Hunton Limestone marker (shown along line AA' in Figure 2) through coherence volumes generated using (a) semblance, and (b) energy-ratio algorithms using analytic traces and the same 5-trace by 20-ms analysis window oriented along structural dip. Green arrows indicate zones of improved fault continuity using energy-ratio coherence. Red arrows indicate zones of greater noise in the semblance coherence. Overall, the energy-ratio coherence slices exhibit crisper, more detailed lineaments than the semblance coherence for this geologic formation. (Data courtesy: TGS, Houston)

338x190mm (230 x 230 DPI)

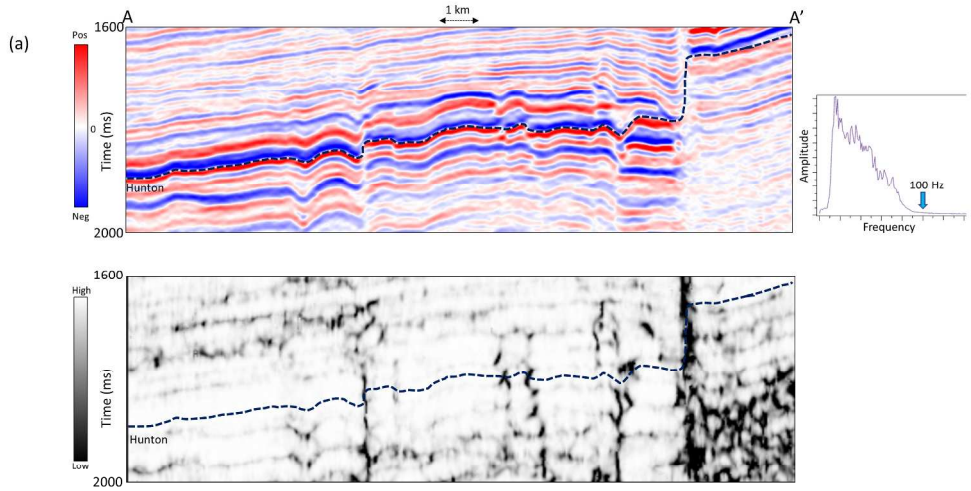

Figure 2a

Figure 2a: Vertical slices along line AA' (top) the original 3D seismic volume and (bottom) the corresponding coherence volume. The spectrum ranges between 10 and 80 Hz but is biased towards the low frequencies. The black dashed-line indicates the top of the Hunton Limestone. (Data courtesy: TGS, Houston)

338x190mm (230 x 230 DPI)

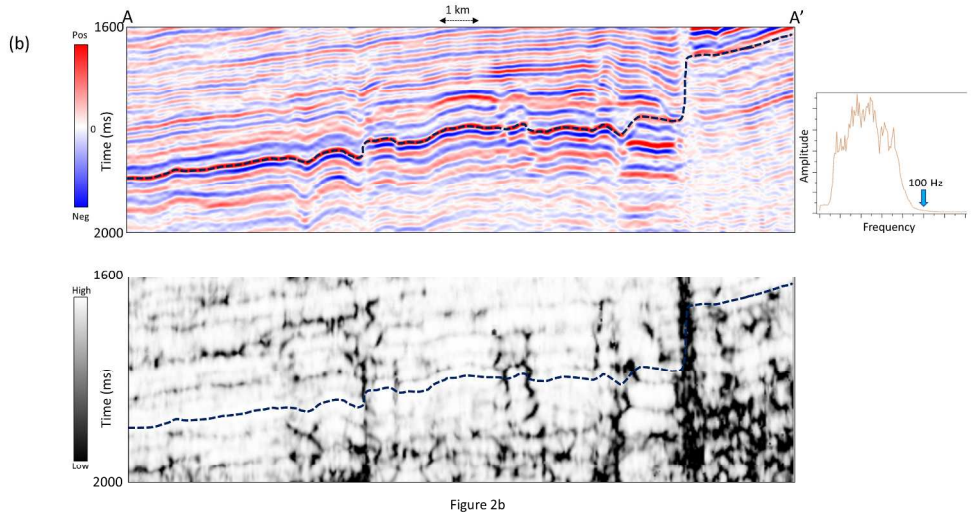

Figure 2b

Figure 2b: Vertical slices along line AA' through (top) the first derivative of the seismic amplitude and (bottom) the corresponding coherence volume. The effect of the first derivative is to flatten the spectrum in the 10-80 Hz range of the signal. (Data courtesy: TGS, Houston)

338x190mm (230 x 230 DPI)

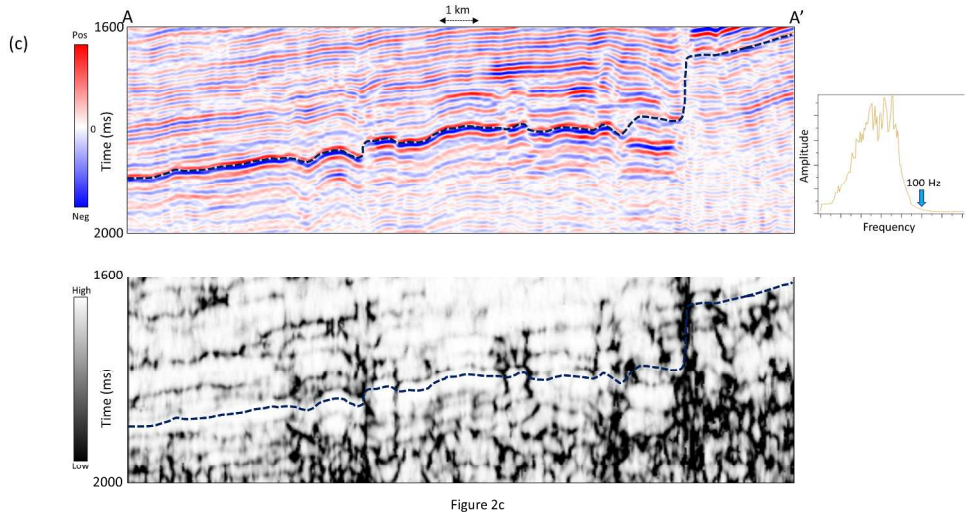

Figure 2c

Figure 2c: Vertical slices along line AA' through through (top) the second derivative of the seismic amplitude and (bottom) the corresponding coherence volume. The effect of the second derivative is to skew the spectrum towards the higher frequencies in the 10-80 Hz range of the signal. (Data courtesy: TGS, Houston)

338x190mm (230 x 230 DPI)

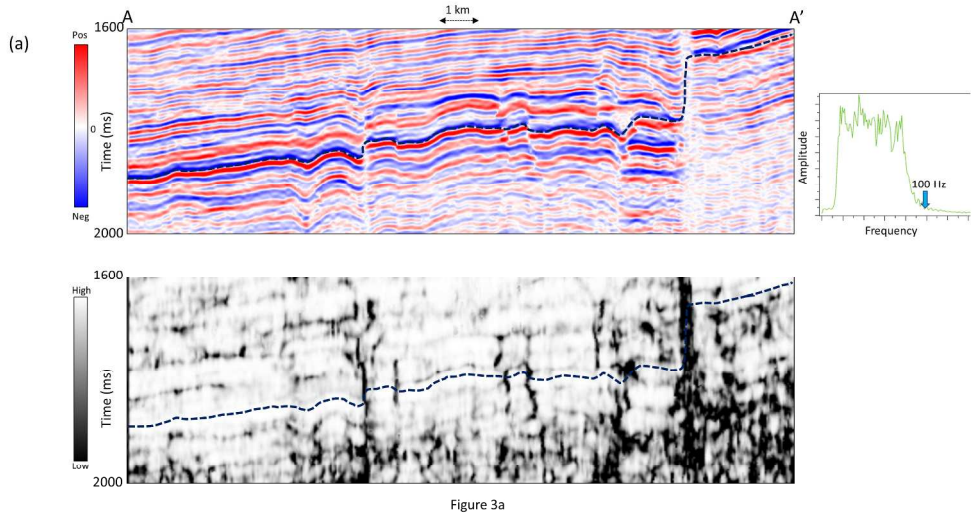

Figure 3a

Figure 3a: Vertical slices along line AA' through through (top) seismic amplitude after spectral balancing 10-20-70-80 Hz using Helmore's (2009) workflow and (bottom) the corresponding coherence volume. Unlike derivative operators, spectral balancing preserves the original phase of each spectral component. (Data courtesy: TGS, Houston)

338x190mm (230 x 230 DPI)

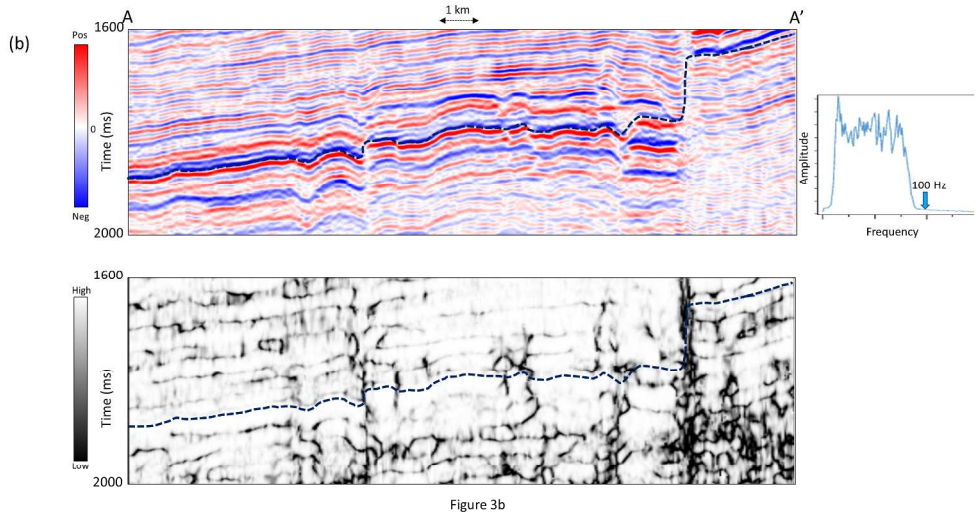

Figure 3b

Figure 3b: Vertical slices along line AA' through through (top) seismic amplitude after spectral balancing to 10-20-70-80 Hz using thin-bed reflectivity inversion and (bottom) the corresponding coherence volume. (Data courtesy: TGS, Houston)

338x190mm (230 x 230 DPI)

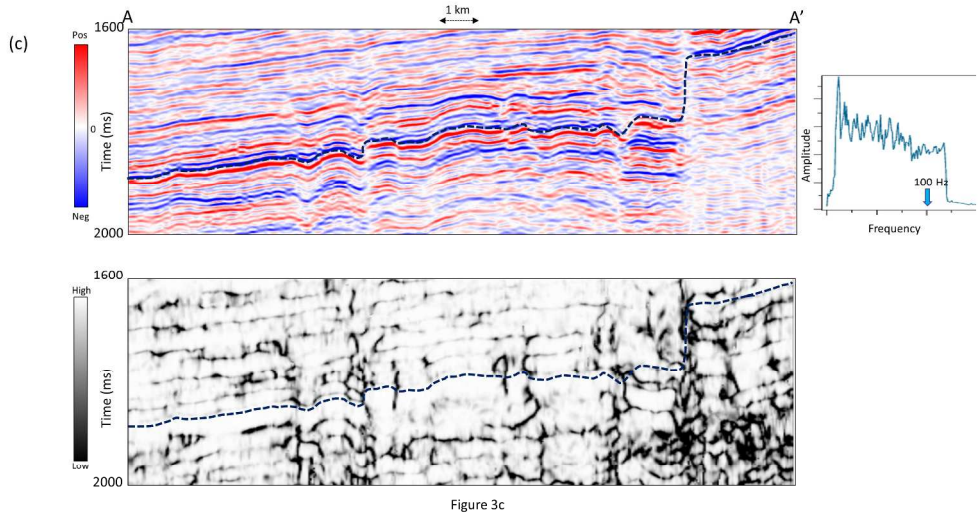

Figure 3c

Figure 3c: Vertical slices along line AA' through through (top) seismic amplitude after bandwidth extension to 10-20-110-120 Hz and (bottom) the corresponding coherence volume. (Data courtesy: TGS, Houston)

338x190mm (230 x 230 DPI)

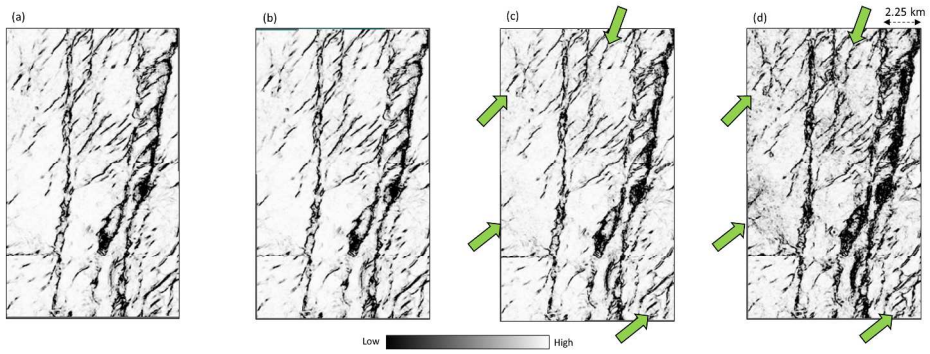

Figure 4

Figure 4: Stratal slices just above the Hunton marker through coherence volumes generated from (a) the original seismic amplitude data, and the seismic amplitude data after (b) structure-oriented filtering, (c) application of the first derivative (b), and (d) application of the second derivative. (b). Green arrows indicate fault details in coherence computed from the first and second derivative amplitude volumes that we interpret to be associated with the lower frequencies. (Data courtesy: TGS, Houston)

338x190mm (230 x 230 DPI)

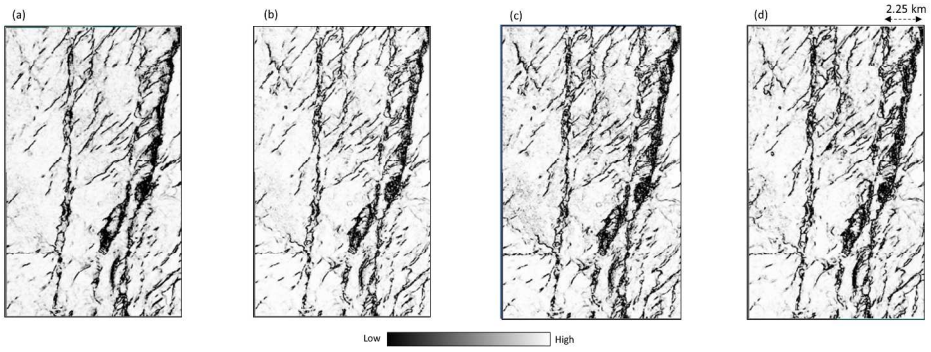

Figure 5

Figure 5: Stratal slices just above the Hunton marker through coherence volumes generated from (a) the original seismic amplitude data, with spectral balancing using Helmore's (2009) workflow, (b) spectral balancing using thin-bed reflectivity inversion, (c) spectral balancing using thin-bed reflectivity inversion subsampled to half sample interval, and (d) bandwidth extension using thin-bed reflectivity inversion to 10-20-110-120 Hz. Notice, spectral balancing bring out more discontinuity detail in the display. Subsampling input seismic data as well as bandwidth extension using thin-bed reflectivity extract even greater detail on these images. (Data courtesy: TGS, Houston)

338x190mm (230 x 230 DPI)

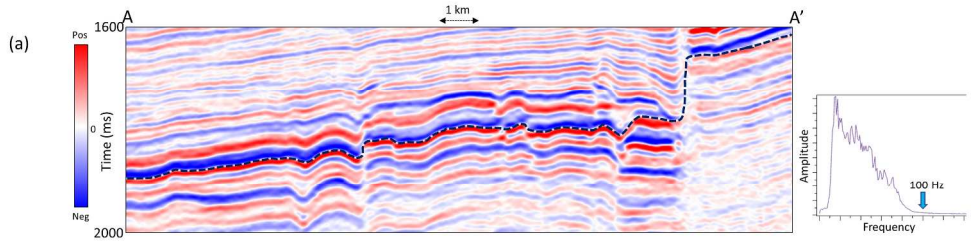

Figure 6a: Vertical slices along line AA' through (a) the original seismic volume, (b) Amplitude Volume Transform (AVT) volume, and (c) the equivalent line through the coherence volume on AVT volume. The AVT extends both the high and low frequency content of the original data, whereby the lower frequencies provide a pseudo-relief or "outcrop" appearance favored by many interpreters. The amplitudes of lower frequencies are higher than those for the higher frequencies, and thus it does give a low frequency look. (Data courtesy: TGS, Houston)

338x190mm (230 x 230 DPI)

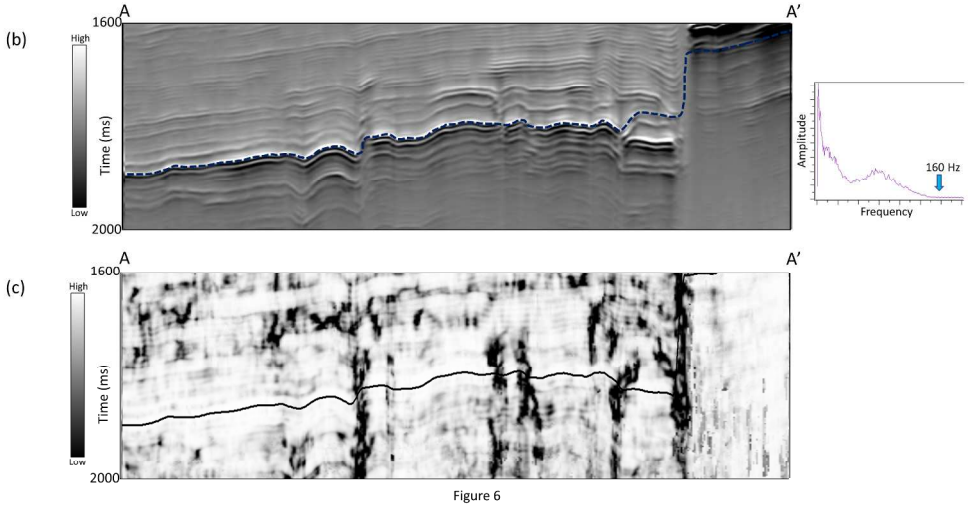

Figure 6

Figure 6bc: Vertical slices along line AA' through (a) the original seismic volume, (b) Amplitude Volume Transform (AVT) volume, and (c) the equivalent line through the coherence volume on AVT volume. The AVT extends both the high and low frequency content of the original data, whereby the lower frequencies provide a pseudo-relief or "outcrop" appearance favored by many interpreters. The amplitudes of lower frequencies are higher than those for the higher frequencies, and thus it does give a low frequency look. (Data courtesy: TGS, Houston)

338x190mm (230 x 230 DPI)

Figure 7

Figure 7: Stratal slices just above the Hunton marker through coherence volumes generated from the AVT volume. This image emphasizes the larger, through-going faults seen by the lower frequencies, and is thus complementary to images obtained using spectral balancing and bandwidth extension. (Data courtesy: TGS, Houston)

338x190mm (230 x 230 DPI)